

Nonlocal electron kinetics and densities of excited atoms in S and P striations

Yu. B. Golubovskii,¹ R. V. Kozakov,¹ V. A. Maiorov,¹ J. Behnke,² and J. F. Behnke²

¹*St. Petersburg State University, St. Petergof, Ulianovskaia 1, 198904 St. Petersburg, Russia*

²*Institute for Physics, Ernst-Moritz-Arndt-University Greifswald, Domstrasse 10A, 17487 Greifswald, Germany*

(Received 15 November 1999; revised manuscript received 22 February 2000)

A numerical solution of the Boltzmann kinetic equation involving elastic and inelastic collisions as well as spatial gradients along the electric field is obtained for the experimentally measured fields in S and P striations. The peculiarities of formation of the distribution function are analyzed. They are connected with the displacements of one distinctive peak in the electron distribution function (EDF) for S striations or two peaks for P striations in accordance with the resonance trajectories. A descriptive model is constructed for the processes of excitation of neon $2p^53s$ and $2p^53p$ atomic states and ionization in striations. The presence of phase shifts between ionization rate and electron density is shown, which can cause ionization wave propagation. Measurements and calculations of the excited state densities are carried out for different striation phases. Comparison of theory and spectroscopic measurements shows a good description of fast electrons by the distribution function in striations. Comparison of theory and probe measurements of the distribution function shows that the main features of the EDF in an energy range below the excitation threshold are experimentally observed.

PACS number(s): 52.35.-g, 52.25.Dg, 52.70.Kz, 52.80.Hc

I. INTRODUCTION

The stratification of the positive column of a glow discharge, i.e., the existence of a discharge in the regime of standing or moving ionization waves (striations), is a striking example of the self-organization of a strongly nonequilibrium system, such as a gas discharge plasma sustained by an electric field. Detailed reviews of experimental and theoretical investigations of striations were published at the end of the 1960s in [1–3]. At that time the striations were understood as waves of ionization-diffusion nature in contrast to numerous other wave instabilities occurring in gas discharge plasmas. Interpretation of the mechanisms of origin and propagation of striation was based upon hydrodynamic models, including charged particle balance equations, momentum transfer equations for electrons and ions, energy balance equations, etc. The range of applicability of fluid models is limited by high pressures and (or) large currents, when due to collisions of various kinds (elastic, inelastic, electron-electron) the electron distribution function (EDF) is formed locally in each striation phase as a function of the electric field. The electron component of a plasma can be described appropriately in terms of the local density, mean energy, diffusion, thermodiffusion, mobility coefficients, etc. However, at low pressures and small currents, where most theoretical and experimental studies applied, the fluid models are inapplicable for description of gas discharge stratification. When the energy relaxation length exceeds the striation length, the distribution function is not formed by the local field, but by the whole potential profile of a striation. Therefore, consideration of the electron fluxes in terms of diffusion, thermodiffusion, and mobility is invalid and consecutive kinetic analysis of the plasma electron component is required.

In inert gases at low pressures and small currents various types of striations are observed. Striations of S type are characterized by a potential drop U_S , slightly exceeding the ex-

citation threshold U_{ex} . Their length L_S is a little larger than $L_0 = U_{ex}/E_0$ (E_0 is the period averaged electric field). The potential drop U_P and length L_P of P -type striations are half the corresponding values of S -type striations.

The stratification of a gas discharge under these conditions is caused by resonance kinetic effects, connected with the specifics of electron movement in an electric field when the energy balance is controlled mainly by inelastic collisions. The picture of electron movement can be represented in the following way. Let an arbitrary distribution function be injected into the homogeneous field E_0 . If the energy loss in elastic collisions is neglected and the presence of only one excitation level is considered, then the electrons being accelerated in the axial field acquire a kinetic energy U under conservation of their total energy $\varepsilon = U + e\varphi(x) = \text{const}$ [$e\varphi(x)$ is the potential energy of an electron in the striation field]. When the kinetic energy attains the excitation threshold U_{ex} , electrons undergo inelastic collision, jump onto the line $\varepsilon - U_{ex} = \text{const}$, and continue their movement until their kinetic energy becomes U_{ex} again, so the picture of movement reproduces itself. On the plane (ε, x) a “staircase” with length L_0 in spatial coordinate and height U_{ex} in energy is forming. Under the above-stated assumptions the electron trajectories do not intersect and the initial distribution function is reproduced for an unlimited distance.

A small energy loss in elastic collisions and the presence of a discrete spectrum of excitation levels located close to each other result in the appearance of a downward flux in energy space. Moreover, electron trajectories intermix, information about the initial EDF is lost, and a homogeneous EDF, determined by the energy gain in the field E_0 and the energy loss in elastic and inelastic collisions, forms at sufficiently long distance.

The relaxation of the initial electron distribution function in a homogeneous field has the form of damped oscillations. Their spatial period L exceeds the length L_0 by the value ΔL ,

determined by the energy loss in elastic collisions at the striation length.

When an arbitrary distribution function is injected into a spatially periodic inhomogeneous field with spatial period L , electron bunching takes place. After a few periods, the initial EDF is compressed into distinct maxima, which move on the plane (ε, x) along resonance trajectories determined by the average energy loss in elastic ΔU_{el} and inelastic $U_{inel} = U_{ex} + \Delta U_{inel}$ collisions on the period of the striation (U_{ex} is the first excitation threshold, and ΔU_{inel} is the small addition to the energy loss connected with the existence of discrete spectrum of excitation levels). The potential drop in one period, $U_L = \int_0^L E(x) dx$, is equal to $U_L = U_{ex} + \Delta U_{el} + \Delta U_{inel}$. The self-consistent electric field is determined by the ion continuity equation, where density and ionization sources are calculated from the electron distribution function. The EDF corresponding to the resonance trajectory leads to a spatial periodicity of ionization sources and, consequently, to spatial periodicity of the field.

If an electron at the resonance trajectory after one spatial period L gains energy U_L larger than the excitation threshold U_{ex} , an S striation of length L_S and potential drop U_S forms. It is also possible that U_L is smaller than U_{ex} . Here the electron has to pass at least two spatial periods in accordance with the resonance trajectory before undergoing an inelastic collision. In this case a P striation is formed, with $L_P = L_S/2$ and $U_P = U_S/2$. There are two resonance trajectories for P striation, which are distanced from each other in total energy by the value $U_{ex}/2$.

A similar picture of S and P striation formation in the positive column of an inert gas discharge has been discussed in a series of papers. The first mentioning spatial resonance phenomena in electron kinetics appeared at the beginning of the 1970s [4–6]. In [7,8], the possibility of existence of a periodic solution of the Boltzmann kinetic equation in a homogeneous field was shown. The distribution function was represented as the product of an amplitude, depending on total energy, and a homogeneous electron distribution, depending on kinetic energy. A recurrence relation for the amplitude was obtained, which was employed in calculating the length and potential drop of S and P striations. In [9] the relaxation of the distribution function in arbitrary fields was investigated by expansion of the required solution with respect to the small parameter $\Theta = (m/M)(U_{ex}/eE_0L)^2$. This permitted an equation for EDF amplitude to be obtained that described the spatial evolution of an arbitrary distribution function in various fields. In particular, it was shown that in spatially periodic fields a bunching effect of electrons takes place. The bunching effect results in the formation of narrow peaks in the distribution function, which move along the resonance trajectories. In [10] the analytical theory given in [9] was generalized by taking inelastic collisions into account. Experimental investigations of the EDF in S and P striations and comparison with the analytical solution of the kinetic equation were performed in [11].

In [12,13] relaxation of the EDF injected into a homogeneous electric field was investigated by numerically solving the kinetic equation. Electron heating in the longitudinal field, energy loss in elastic collisions, excitation of several levels, and ionization processes were considered. The investigation showed that in a certain range of electric field

strengths an explicit periodic solution with small damping exists. It was also shown that, when the values of E_0/p are small, the damping is caused by energy loss in elastic collisions, and at large values of E_0/p it is caused by excitation of several upper levels of the inert gas atom.

A detailed investigation of the establishment of the EDF in homogeneous as well as S - and P -striation-like fields by numerically solving the kinetic equation was carried out in [14]. The role of various processes was elucidated, in particular, the role of energy loss in elastic collisions and excitation of several discrete states during the relaxation of the initial EDF in homogeneous fields and sinusoidally modulated resonance fields. In [15] the phase shifts between the field, electron density, and excitation and ionization rates were calculated in dependence on the degree of field modulation. It was shown that unexpectedly large phase shifts between the field and rates of excitation and ionization occur, which are connected with the energy gain in the potential field of striation and the small energy loss in elastic collisions. The possibility of an explanation of ionization wave propagation with the help of these phase shifts was mentioned.

In the present paper the excitation processes of neon levels $2p^53s$ and $2p^53p$ as well as ionization processes are studied in experimentally measured fields on the basis of nonlocal electron kinetics. A detailed picture of physical processes occurring in S and P striations is constructed. Measurements of the excited state densities are performed. The comparison of theory and spectroscopic experiments gives information about the formation of the distribution function in the high energy domain. The comparison of theory and probe measurements gives information about the form of the distribution function of the electrons at energies lower than the excitation threshold.

II. NONLOCAL ELECTRON KINETICS IN S AND P STRIATIONS

Detailed studies of distribution function formation in sinusoidally modulated striation-like fields, taking the spatial gradients into account, were carried out in [14,15]. The real field of S and P striations differs considerably from a sinusoidally modulated one. Correct measurements of the potential profile in striations by simultaneous movement of the cathode and anode relative to the fixed probe [16] or by moving the probe when both cathode and anode locations are fixed [11] allow one to exclude the integral plasma oscillations and to obtain the potential distribution in space and time. In Fig. 1 the potential distributions measured in [11] and the field distributions are shown for S (a) and P striations (b). There are comparably narrow regions of strong field and extensive regions of weak field. Therefore, a great difference between the measured field and a sine-modulated one can be seen. The analytical solution of the kinetic equation in such fields under the ‘‘black wall’’ approximation at the excitation threshold and neglecting the inelastic collisions was reported in [11,17]. In the present paper numerical calculations of the distribution function are carried out for measured potential fields. The rates of excitation and ionization will be calculated with the help of those distribution functions and a picture of the physical processes occurring in striations will be constructed.

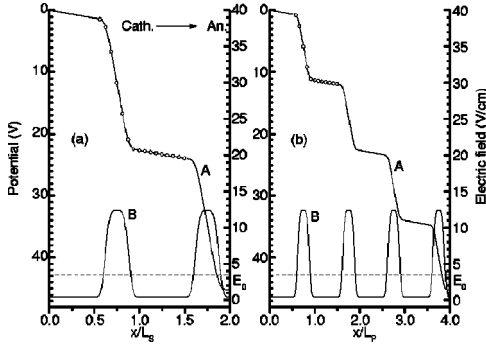


FIG. 1. The axial distribution of the potential $\varphi(x)$ (curve A, left scale) and the field $E(x)$ (curve B, right scale), measured in S striation (a) and P striation (b) in neon ($p=2.7$ torr, $i=5$ mA, $R=1$ cm). The dashed curve denotes the mean electric field. The phases of the striations where the calculated and measured distribution functions were compared (Figs. 6 and 7 below) are marked by dots.

The parameters of regular striations that have been observed in neon discharge at low pressures $p=2-3$ Torr and small currents $i=5$ mA in a tube with radius $R=1$ cm are given in Table I. This shows that the striation length appears to be considerably shorter than the energy relaxation length with respect to elastic collisions, $\lambda_e \sim \lambda \sqrt{M/m}$, and the striation period much exceeds the typical time τ of EDF establishment. In fact, the establishment time of the isotropic part of the EDF due to elastic collisions with frequency ν has the value $M/(m\nu) \sim 10$ μ sec, and the time of acquisition of the excitation energy U_{ex} equals $(U_{ex}/eE_0)(m\nu/eE_0) \sim 2$ μ sec. Thus at low pressures and small currents the fastest process of EDF temporal establishment is the energy gain in a field up to the excitation threshold, with subsequent inelastic collision. At the same time this process determines the typical spatial scale of the field periodicity L_0 . Consequently, as $\lambda_e > L_{S,P}$, the EDF is not being formed by the local field in each phase of the striation, but by the whole potential profile. By virtue of the relation $\tau \ll T_{S,P}$ it is possible to neglect the time derivative in the kinetic equation.

The steady-state kinetic equation for the distribution function $f(\vec{v}, \vec{r})$ in the variables (\vec{v}, \vec{r}) has the form

$$\vec{v} \cdot \nabla_{\vec{r}} f + \frac{e}{m} \vec{E} \cdot \nabla_{\vec{v}} f = S^{el}(f) + \sum_k S_k^{in}(f), \quad (1)$$

where \vec{E} is the inhomogeneous field, S^{el} is the operator of elastic collisions, and S_k^{in} is the operator of conservative inelastic collisions with consequent excitation of the k th atomic level. Assuming the field $\vec{E}(x)$ to be parallel to the x

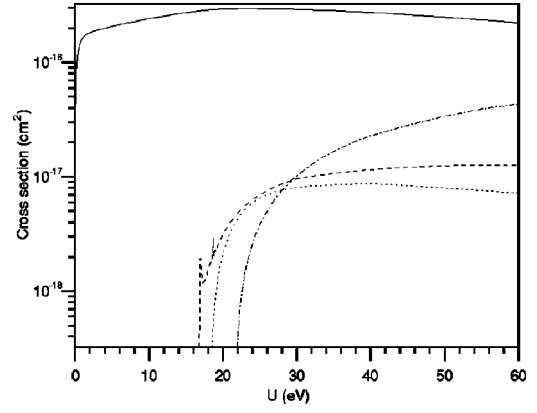


FIG. 2. Cross sections of elastic collisions Q^{el} (solid curve), excitations of S series Q_S^{in} (dashed curve) and P series Q_P^{in} (dotted curve), and ionization Q_I^{in} (dash-dotted curve) in neon [18].

axis and the EDF to be weakly anisotropic, a two-term expansion in Legendre polynomials gives ($U = mv^2/2$)

$$f\left(U, \frac{v_x}{v}, x\right) = \frac{1}{2\pi} \frac{1}{(2/m)^{3/2}} \left(f_0(U, x) + f_1(U, x) \frac{v_x}{v} \right). \quad (2)$$

Substitution of the expansion (2) into Eq. (1) and introduction of the total energy $\varepsilon = U - \int_0^x eE(x') dx'$ yield an equation for the isotropic part of the EDF in a form suitable for numerical solution [12]:

$$\begin{aligned} & \frac{\partial}{\partial x} \left(\frac{U}{3NQ^\Sigma(U)} \frac{\partial f_0(\varepsilon, x)}{\partial x} \right) \\ & + \frac{\partial}{\partial \varepsilon} \left(2 \frac{m}{M} U^2 N Q^{el}(U) f_0(\varepsilon, x) \right) \\ & = \sum_k U N Q_k^{in}(U) f_0(\varepsilon, x) - \sum_k (U + U_k) N \\ & \quad \times Q_k^{in}(U + U_k) f_0(\varepsilon + U_k, x), \end{aligned} \quad (3)$$

where Q^Σ denotes the total transport cross section of electron-atomic collisions, including the cross section of elastic collisions Q^{el} and cross sections of inelastic processes Q_k^{in} of excitation of the level k with the energy U_k . The transport cross sections of collision processes used to solve Eq. (3) are shown in Fig. 2.

Equation (3) with the boundary conditions

TABLE I. The parameters of regular striations in neon discharge, $i=5$ mA, $R=1$ cm. P is the pressure, L is the spatial period, E_0 is the mean electric field, U_L is the fall of the potential in the period, T is the temporal period, and $v_{ph}=L/T$ is the phase velocity of striation.

Type	P (Torr)	L (cm)	E_0 (V/cm)	U_L (eV)	T (μ sec)	v_{ph} (m/sec)
S	3	5.1	3.69	18.9	350	146
P	2	2.5	3.81	9.5	700	36

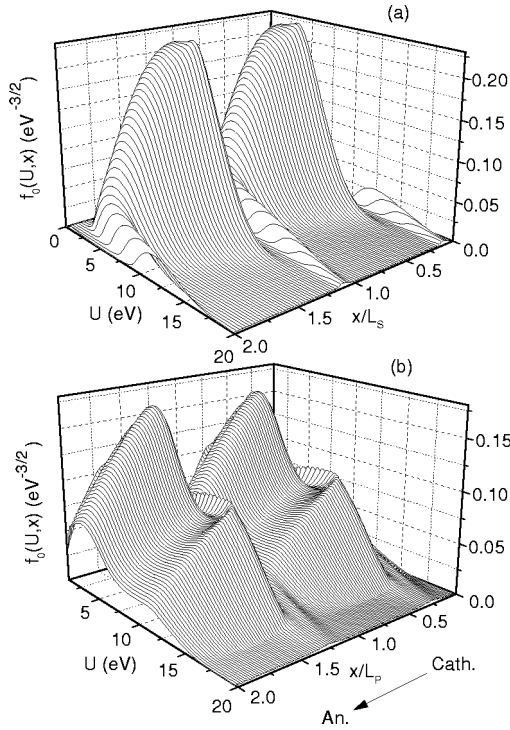


FIG. 3. The electron distribution functions in dependence on kinetic energy U and reduced coordinate x/L for S striation (a) and P striation (b), calculated under conditions represented in Fig. 1.

$$f_0(\varepsilon, x)|_{x=0} = f_0^{(0)}(U),$$

$$\left. \frac{\partial f_0(\varepsilon, x)}{\partial x} \right|_{U=0} = 0, \quad (4)$$

$$f_0(\varepsilon, x)|_{U \rightarrow \infty} = 0$$

was solved for a neon discharge in the inhomogeneous field shown in Fig. 1 using the technique of Ref. [12]. The Crank-Nicholson scheme with an equidistant grid in the spatial coordinate x and a nonequidistant grid in total energy ε was applied to solve the equation. The distribution function was calculated on many potential periods and the established solution was taken as the result.

The kinetic equation in the form (3) can be considered as the continuity equation for divergence of a flux on the plane (ε, x) (left-hand side of the equation) with sinks of high-energy electrons due to inelastic collisions (first term on the right-hand side) and sources of slow electrons (backscattering, second term on the right-hand side). At low pressures the component of flux along the x axis (first term on the left-hand side) greatly exceeds the drift downward in energy space due to elastic collisions (second term on the left-hand side). The order of magnitude of the ratio of flux components is determined by the parameter $(\Theta = m/M)(U_{ex}/eE_0\lambda)^2 \sim (L/\lambda_e)^2$. In [9] the smallness of this parameter was used to obtain an analytical solution of Eq. (3) in arbitrary fields, under the approximation of a “black wall” at the excitation threshold, by expansion with respect to this small parameter.

In the present paper a numerical solution of Eq. (3) is obtained. This solution in the form of a three-dimensional (3D) plot is represented in Fig. 3 for S (a) and P striations

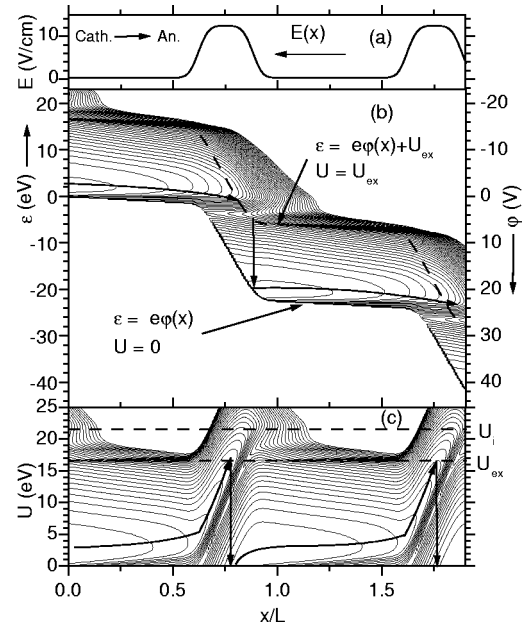


FIG. 4. The contour plots for EDF's in S striation correlated with electric field; (a) the electric field as a function of reduced coordinate x/L ; (b) contour plot in variables of total energy ε and reduced coordinate; (c) contour plot in variables of kinetic energy U and reduced coordinate. Arrows show the resonance trajectories along which the typical peaks in the EDF move. The values of kinetic energy corresponding to potentials of excitation of the lowest atomic level and ionization are marked by dashed curves. The conditions of the calculation are represented in Fig. 1.

(b). The contour plots [lines of constant level, along which $f_0(\varepsilon, x) = \text{const}$ or $f_0(U, x) = \text{const}$] are shown in Fig. 4 for S striation and in Fig. 5 for P striation. Figures 3(a) and 3(b) give a general representation of the spatial structure of distribution functions in S and P striations. Qualitative consid-

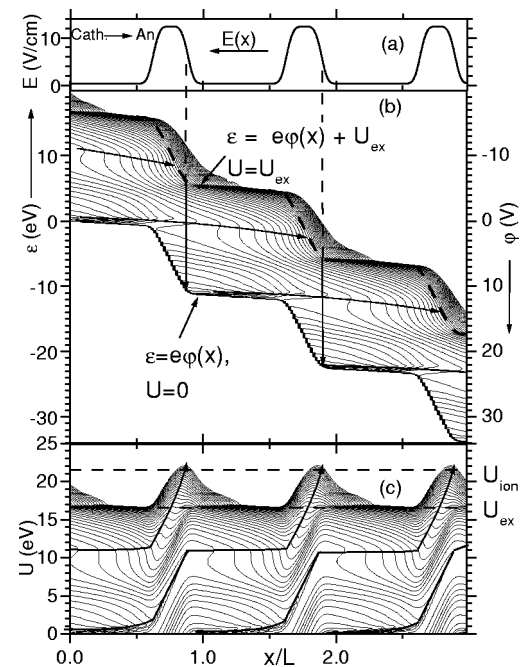


FIG. 5. The contour plots for EDF's in P striation correlated with electric field. The notation is the same as in Fig. 4.

TABLE II. Actual and effective phase shifts between the maxima of the field and density $\Delta(E,n)$, excitation $\Delta(E,W)$, and ionization $\Delta(E,I_d)$, and those between the maxima of the density and excitation $\Delta(n,W)$ and ionization $\Delta(n,I_d)$ for S and P striations.

	$\Delta(E,n)$	$\Delta(E,W)$	$\Delta(E,I_d)$	$\Delta(n,W)$	$\Delta(n,I_d)$
S , actual	0.17	1.047	1.095	0.877	0.92
P actual	0.175	2.098	2.117	1.923	1.942
S , eff.	0.17	0.047	0.095	-0.123	-0.08
P , eff.	0.175	0.098	0.117	-0.077	-0.058

erations about the formation of such distribution functions can be obtained from Figs. 4 and 5.

On the plane (ε, x) for S striation the displacement of the sole typical maximum in the distribution function in the domain of elastic collisions $0 < U < U_{ex}$ in accordance with the resonance trajectory is indicated by the arrow (Fig. 4). When the kinetic energy attains the excitation threshold, this maximum jumps onto the line $\varepsilon - U_{ex} = \text{const}$ and moves again along the resonance trajectory. The compression of the distribution function into typical maxima, moving along the resonance trajectories, is caused by the electron bunching effect in a spatially periodic resonance field shown in Fig. 1(a). The transition from the variables (ε, x) [Fig. 4(b)] to (U, x) [Fig. 4(c)] shows the displacement of the maximum of the distribution function in both kinetic energy space and real space that is distinctly seen in the 3D graph [Fig. 3(a)].

For P striation the structure of the distribution function differs from that of S striation in the presence of two maxima, also moving along the resonance trajectories [Fig. 5(b)]. Since the potential drop of P striation is smaller than the excitation threshold, electrons have to pass two spatial periods before undergoing an inelastic collision. In Fig. 4(c) it is distinctly seen that two resonance trajectories are formed, along which two typical maxima move on the planes (ε, x) and (U, x) ; maxima movements are shown by the arrows.

An anomalously large phase shift is formed between the fast electrons able to excite or ionize an atom ($U > U_{ex}$), and slow electrons ($U < U_{ex}$) contributing to the electron density. Electrons pass the elastic domain with small energy loss in elastic collisions. The relaxation length in the inelastic domain $\lambda_g^* = \sqrt{\lambda} \lambda^*$ is about 0.2 cm, which is much shorter than a typical scale of the field. That is the reason for local formation of the EDF at the energies $U > U_{ex}$. From Figs. 4 and 5 the phase shifts between the maxima of the field $E(x)$, density $n(x)$, excitation $W(x)$, and direct ionization rate $I_d(x)$ can be determined. In local theory the maxima of excitation and ionization must coincide with the field maxima, and in nonlocal theory their phase shift exceeds the spatial period. This means that excitation and ionization at the point X_{max} are produced by electrons being accelerated in the electric field from the point $X_{max} - L$ for S striation or $X_{max} - 2L$ for P striation. Due to a shift by almost a period, the maxima of excitation and direct ionization rates are imposed upon the phase of electron density increase, which can be a reason for ionization wave propagation.

The actual phase shifts between maxima of the field and density $\Delta(E,n)$, excitation $\Delta(E,W)$, and ionization

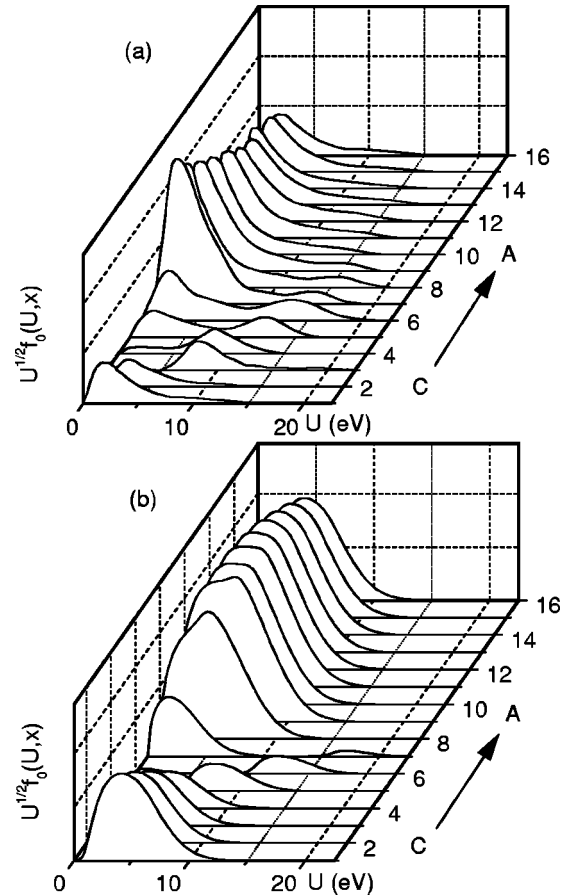


FIG. 6. The comparison of measured (a) and calculated (b) distribution functions in S striation at 16 phase points indicated in Fig. 1(a).

$\Delta(E,I_d)$, as well as between maxima of the density and excitation $\Delta(n,W)$ and ionization $\Delta(n,I_d)$, for S and P striations are represented in Table II. In the same table the effective values of phase shifts (subtracting an integer number of periods), which can be observed in experiment, are also represented.

The comparison of calculated and measured [11] distribution functions in various phases of S and P striations indicated by dots in Fig. 1 is represented in Figs. 6 and 7. From these figures one can see a qualitative agreement between theory and experiment. The experimental results give the typical maxima in the distribution function, shifting along the energy and coordinate axes according to nonlocal theory. Probe measurements of the EDF give information about electrons at not very large energies. Information about the high-energy part of the EDF can be obtained on the basis of spectroscopic measurements of the excited state densities.

III. CALCULATION OF THE $2p^53s$ AND $2p^53p$ STATE DENSITIES IN S AND P STRIATIONS

The distribution functions in S and P striations calculated in the previous section permit us to calculate the excitation rates of each level N_{sk} of the series $2p^53s$ and N_{pj} of the series $2p^53p$, when the cross sections of corresponding processes are known, and, further, to obtain the densities of

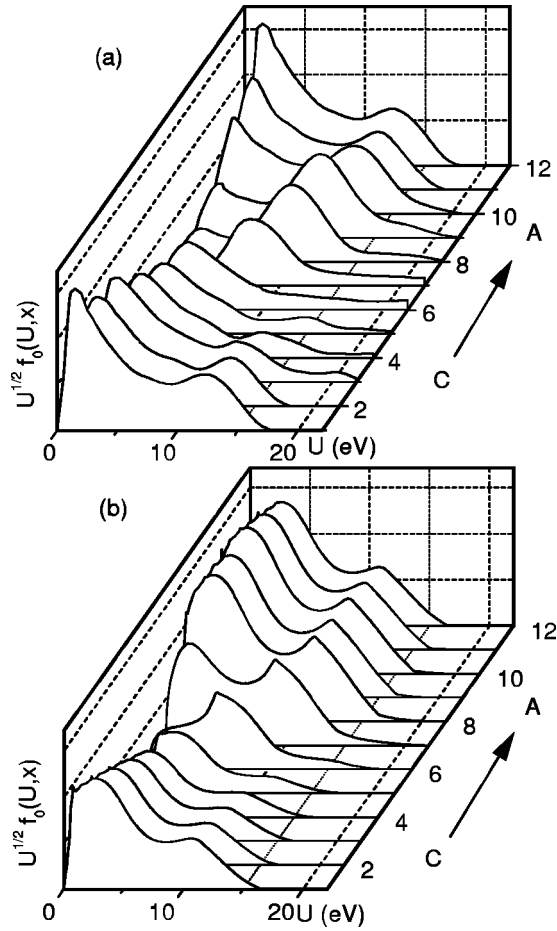


FIG. 7. The comparison of measured (a) and calculated (b) distribution functions of P striation at 12 phase points shown in Fig. 1(b).

these levels using the balance equations. The cross sections of direct and stepwise processes of excitation and ionization by electron collision used in the following calculations were taken from [18–20]. The frequencies of these processes can be obtained by averaging them over the kinetic energy together with the EDF,

$$Z_{p,q}^e(x) = \sqrt{\frac{2}{m}} \int_{U_{p,q}}^{\infty} Q_{p,q}(U) f_0(U, x) U dU. \quad (5)$$

A diagram of the basic processes considered in the calculations is displayed in Fig. 8. The subscripts p and q correspond to the initial and final atomic states (0 is the ground state $2p^6$, sk is the k th level of the series $2p^53p$, pi is the i th level of the series $2p^53s$, and ion denotes the ionization). The superscript e means the process is caused by an electron impact. The lower integration limit $U_{p,q}$ is the threshold of a process. This model is valid for values of electron density that are not extremely high, when the collisional processes of quenching are negligibly small in comparison with the radiative transitions for all excited states, except those of the series $2p^53s$. This is the so-called immediate ionization approximation. The estimation shows the validity of the model for electron densities $n < 10^{14} \text{ cm}^{-3}$.

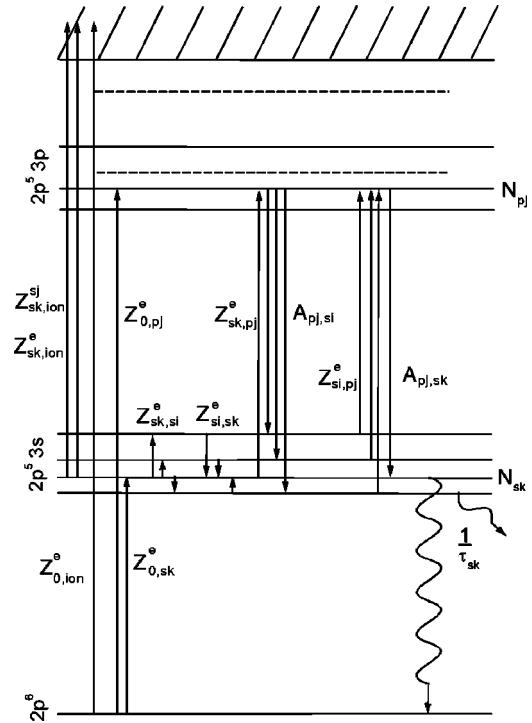


FIG. 8. The diagram of the basic processes for neon. Here N_p is the atom density in state p and $Z_{p,q}^e$ is a constant of collisional transition from state p to state q by electron impact. The states considered are 0 (ground level $2p^6$), sk (k th level of series $2p^53s$), pj (j th level of series $2p^53p$), and ion (state of ionization). $A_{pj,sk}$ is the constant of the radiative transition from j th radiating level to k th absorbing level. $Z_{sk,ion}^e$ is the constant of ionization by collision of two atoms in states sk and sj . τ_{sk} is the effective lifetime the metastable or resonance state.

The metastable state densities can be described by continuity equations in the form

$$\frac{\partial N_M(\vec{r}, t)}{\partial t} + \text{div} \vec{\Gamma}_M = W_M - H_M, \quad (6)$$

where N_M is the density of the metastable state N_{s3} or N_{s5} , $\vec{\Gamma}_M$ is the diffusion flux of the metastable atoms, containing axial and radial components, and W_M and H_M are the rates of excitation and quenching due to collision processes of various kinds, generally depending on spatial and temporal coordinates. The axial distribution of metastable atoms on the discharge axis is of interest; therefore the radial diffusion can be described by the typical lifetime of metastable atoms connected with a diffusion to the wall, $\tau_M \approx (R/2.4)^2/D_M$. This lifetime under the conditions discussed has a value of about 3 ms and exceeds the striation period, so the temporal derivative in Eq. (6) has to be retained. It is possible to neglect the axial diffusion of metastable atoms, since they diffuse during their lifetime for the length ~ 0.4 cm, which is much shorter than the striation length. Consequently, the term $\text{div} \vec{\Gamma}_M$ can be reduced to N_M/τ_M .

The densities of resonance states can be calculated on the basis of the integral equation of radiation transport [21,22],

$$\frac{\partial N_R(\vec{r}, t)}{\partial t} = W_R - H_R - A_{R0} N_R(\vec{r}, t) + A_{R0} \int_{(V)} N_R(\vec{r}', t) K(|\vec{r} - \vec{r}'|) dV', \quad (7)$$

where N_R is the density of the resonance state N_{s2} or N_{s4} , W_R and H_R are the rates of excitation and quenching in collision processes of various kinds, and A_{R0} is the probability of spontaneous emission. The integral on the right-hand side of Eq. (7) describes the production rate of excited resonance atoms at the point \vec{r} due to absorption of the resonance quanta emitted at the point \vec{r}' . The integration is carried out over the whole discharge volume. Since the absorption coefficient in the spectral line wings is small, the quanta with these frequencies can pass large distances without any absorption; therefore Eq. (7) cannot be reduced to a diffusion equation similar to Eq. (6). The great simplification of Eq. (7) is connected with the abruptly decreasing dependence of the core $K(\rho)$ on its argument. If the spatial distribution of resonance atoms is flat enough, that is, the function $N_R(\vec{r}')$ changes weakly at the core $K(|\vec{r} - \vec{r}'|)$ scale, the density $N_R(\vec{r}')$ can be factored out from the integral at the point \vec{r} . In this approximation it is possible to introduce an effective lifetime of resonance atoms τ_{eff} [21,22], which depends on the discharge geometry and the spectral line contour; in particular, on the absorption coefficient at the line center. Then for axial distribution of the resonance atoms the last two terms in Eq. (7) are reduced to N_R / τ_{eff} . This expression is similar to those for metastable atoms.

The absorption coefficients at the line center at $N_0 \sim 10^{17} \text{ cm}^{-3}$ can vary in the range $(3-50) \times 10^4 \text{ cm}^{-1}$ for the level $s2$ and $(3-50) \times 10^3 \text{ cm}^{-1}$ for the level $s4$. The value of the absorption coefficient depends on the type of spectral line profile. At such large absorption coefficients the resonance radiation propagates in the distant Lorentzian wings of the spectral lines. The width of the Lorentzian profile is a combination of the intrinsic width and the broadening originating from collisions between the atoms. For a singlet-singlet transition the constant of collisional broadening much exceeds that for a triplet-singlet transition. Therefore the parameters of the Voigt profile for the transitions $3^1P_1 - 2^1S_0$ and $3^3P_1 - 2^1S_0$ differ greatly, and resonance radiation trapping can result in different decreases of spontaneous emission probabilities for different resonance lines. As the analysis of experimental data shows, satisfactory values for the effective probabilities of transitions are $A_{eff} \approx 10^6 \text{ sec}^{-1}$ for the transition $3^1P_1 - 2^1S_0$ and $A_{eff} \approx 10^4 \text{ sec}^{-1}$ for the transition $3^3P_1 - 2^1S_0$.

For excited atoms in the emitting states $2p^53p$, the temporal and spatial derivatives can be neglected, since the spontaneous emission lifetime is extremely small and atoms radiate at the same point and instant where they were excited.

Following the above simplifications, the balance equations for the densities of the k th level N_{sk} of the series $2p^53s$ and i th level N_{pi} of the series $2p^53p$ in accordance with the diagram in Fig. 8 have the form

$$\frac{\partial N_{sk}}{\partial t} = N_0 Z_{0,sk}^e + \sum_{j \neq k} N_{sj} Z_{sj,sk}^e + \sum_{j=1}^{10} N_{pj} A_{pj,sk} - N_{sk} \left(\sum_{j \neq k} Z_{sk,sj}^e + \sum_{j=1}^{10} Z_{sk,pj}^e + Z_{sk,ion}^e + \frac{1}{\tau_{sk}} + \sum_{j=2}^5 Z_{sk,ion}^{sj} \right), \quad k=2,3,4,5; \quad (8)$$

$$N_0 Z_{0,pi}^e + \sum_{j=2}^5 N_{sj} Z_{sj,pi}^e = N_{pi} \sum_{j=2}^5 A_{pi,sj}, \quad i=1,2, \dots, 10. \quad (9)$$

The first three terms on the right-hand side of Eq. (8) correspond to the population of the level N_{sk} from direct excitation from the ground state, electron impacts in the series $2p^53s$, and radiating transitions from the series $2p^53p$. The terms in large parentheses on the right-hand side describe the quenching of this level by means of electron impact inside the series $2p^53s$, stepwise transition into the series $2p^53p$, stepwise ionization, decay caused by the finite lifetime, and ionization due to collisions with excited atoms s_j (chemoionization). The lifetime finiteness for the metastable states N_{s3} and N_{s5} is stipulated by their diffusion to the wall and that for the resonance states N_{s2} and N_{s4} is caused by the escape of resonance radiation taking account of radiation trapping in the volume. The constants of intermixing processes in the series of lower s levels by collisions with the neutral atoms $Z_{sk,sj}^0$ can be found in [23]. At the low pressures being considered these processes can be neglected. The constants of intermixing processes by electron impact $Z_{sk,sj}^e$ were taken from [25].

The left-hand side of Eq. (9) contains the processes of direct and stepwise excitation of the level N_{pi} of the series $2p^53p$, which are balanced by radiative transition into lower levels. The probabilities of radiative transitions $2p^53p \rightarrow 2p^53s$ were taken from [24].

Resolving the system (9) for N_{pi} and substituting these densities into Eq. (8), one can get the system of equations for N_{sk} , which can be written in the form of one vector equation,

$$\frac{\partial \vec{N}_s}{\partial t} + \hat{M} \vec{N}_s = \vec{W}_s. \quad (10)$$

The components of the vector \vec{N}_s are the required densities N_{s2} , N_{s3} , N_{s4} , and N_{s5} of the metastable and resonance levels. The free term vector \vec{W}_s contains the components responsible for direct and cascade (through p levels) excitation of the level N_{sk} . The matrix \hat{M} , called the relaxation matrix, contains the process of direct and cascade intermixing and the escape processes.

Solution of the system of four differential equations (10) using the Runge-Kutta method permits one to obtain the time dependences of the densities N_{sk} . Since the free term is periodic, a periodic solution is establishing after a few temporal periods. The chemoionization processes, which are nonlinear with respect to the density N_{sk} , were considered by a suc-

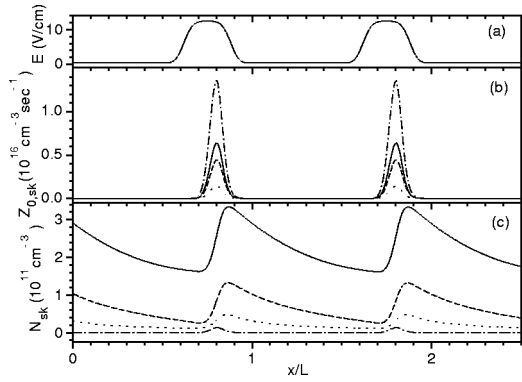


FIG. 9. The calculated densities N_{sk} (c) and excitation rates $Z_{0,sk}^e$ (b) of $2p^53s$ levels in dependence on reduced coordinate x/L , correlated with field (a), for S striation. $s5$, solid curve; $s4$, dashed curve; $s3$, dotted curve; $s2$, dash-dotted curve.

cessive approximation technique. The constants of these processes were taken from [26]. These processes were found to be inessential in the formation of excited state densities.

IV. EXCITATION AND IONIZATION PROCESSES IN S AND P STRIATIONS

The results obtained in previous sections allow us to develop a descriptive picture of the physical processes in striations. In Figs. 9 and 10 the profiles of density (c) and excitation rate (b) of $2p^53s$ levels correlated with a field (a) are represented. Figure 9 describes S striation and Fig. 10 corresponds to P striation. In Figs. 11 and 12 the distributions of excitation rates, both direct and stepwise, for two levels of the series $2p^53p$ (a), as well as the different ionization rates correlated with an electron density (b) are shown for both S and P striation.

The rather narrow regions containing the processes of direct excitation and ionization are typical for both types of striation. They are located within the limits of the strong field domain. It should be kept in mind that the electrons producing excitation and ionization attain the necessary energy at a length a little exceeding the S striation or, correspondingly, doubled P striation length. This feature can be distinctly seen

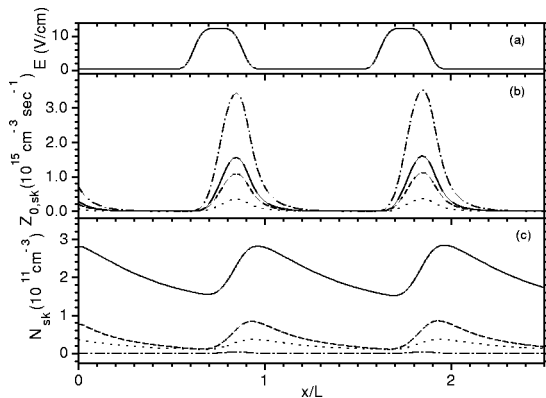


FIG. 10. The calculated densities N_{sk} (c) and excitation rates $Z_{0,sk}^e$ (b) of $2p^53s$ levels in dependence on reduced coordinate x/L , correlated with field (a), for P striation. The curves marked as in Fig. 9.

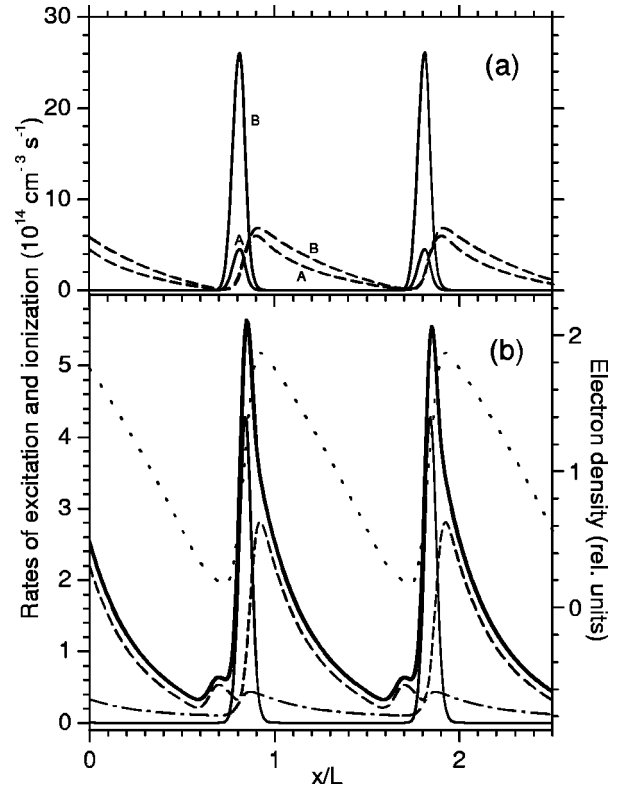


FIG. 11. Rates of various processes in S striation in dependence on x/L . (a) Rates of direct (solid curves) and stepwise (dashed curves) excitation of levels $p7$ (curves A) and $p10$ (curves B) in the system $2p^53p$; (b) rates of direct ionization (solid curve), stepwise ionization (dashed curve), chemoionization (dash-dotted curve), and total ionization (thick curve). Dotted curve in (b) denotes the profile of electron density.

in the contour plots of the EDF on the plane (ε, x) represented in Figs. 4 and 5.

The coincidence of the regions of excitation, ionization, and strong field is stipulated by the short energy relaxation length of fast electrons. The fast electrons produce excitation and ionization at the typical length $\lambda_e^* \sim \sqrt{\lambda\lambda^*}$, which is shorter than the strong field domain. The finite lifetime of the metastable atoms, comparable with a striation period, and the intermixing processes of various kinds result in broadening of the density profiles of $2p^53s$ levels relative to the excitation rate profile [Figs. 9(c) and 10(c)]. The modulation depth of the resonance level 1P_1 appears to be considerably larger but the density much smaller than those of other levels. This is caused by the large effective probability of decay by resonance radiation, in spite of the large value of the direct excitation cross section.

The ratio of the $^3P_{0,1,2}$ state densities at their maxima differs little from that of the statistic weights 1:3:5. For instance, this ratio is 1:2.7:6.8 in S striation [Fig. 9(c)] and 1:2.2:7.5 in P striation [Fig. 10(c)]. This feature indicates intensive intermixing in the series of these levels. In the absence of considerable intermixing, the ratio would be expected to be 1:0.2:5. In fact, the excitation cross sections for the metastable levels 3P_0 and 3P_2 are proportional to their statistic weights, but their diffusion times are nearly identical. The cross section of the resonance level excitation is comparable to that of the level 3P_2 , but the decay time is

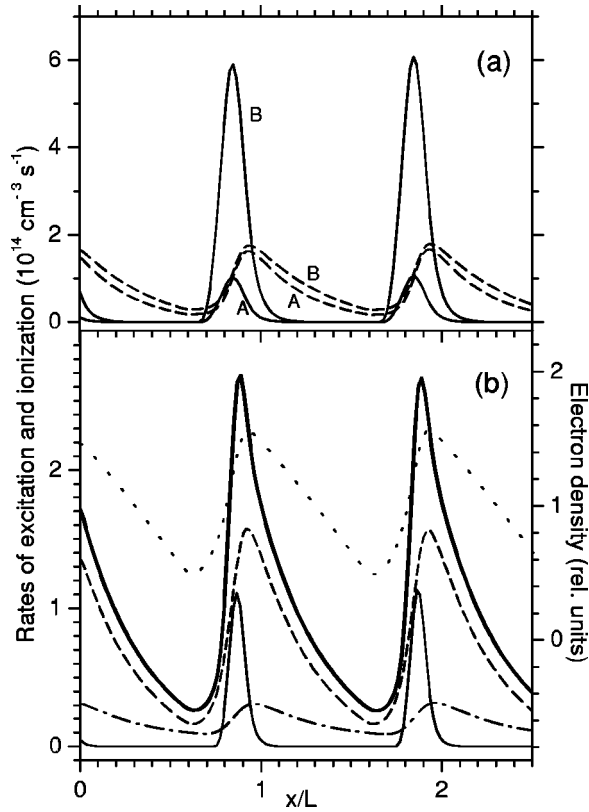


FIG. 12. Rates of various processes in P striation in dependence on x/L . The notation is the same as in Fig. 11.

smaller by a factor 25. The relative densities of the levels ${}^3P_{0,1,2}$ vary along the striation and are related as 1:2.1:13.4 for S striation and 1:1:13.6 for P striation at their minima. Consequently, in the absence of excitation the intermixing leads to population of mostly the lower metastable level 3P_2 . Analysis of the relaxation matrix permits one to point out the main channels of decay of each level. For instance, the metastable states are depleted mainly because of transitions into resonance levels with subsequent resonant radiation escape, but not because of diffusion to the wall.

It is interesting to note that excitation of the levels of the series $2p^53s$ in S striation is approximately twice as intensive as that in P striation, but it is located in a narrower region, which results in approximately identical absolute densities for both types of striation.

The processes of direct and stepwise excitation of radiating levels of the series $2p^53p$ in S striation [Fig. 11(a)] are approximately four times more intense and located in narrower regions than those in P striation [Fig. 12(a)]. The absolute values of direct and stepwise excitation rates are comparable for striations of each type. As is seen from Figs. 11(a) and 12(a), the $2p^53p$ levels are excited by direct processes in a very narrow region, and by stepwise processes they are excited over the whole striation period.

The rates of direct, stepwise, and chemoionization in S and P striations are represented in Figs. 11(b) and 12(b). The profile of the electron density is also shown in the figures by the dashed curve. It is seen from Fig. 11(b) that in S striation the peak of the direct ionization rate exceeds the rate of stepwise ionization in amplitude, being located in a narrower domain. Beyond this domain the ionization is governed by

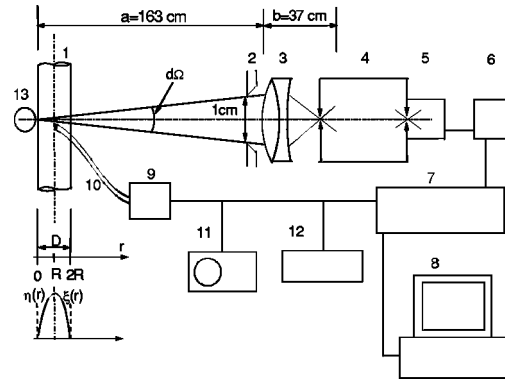


FIG. 13. Scheme of experimental technique for the measurements of the level densities of series $2p^53s$ and $2p^53p$ by methods of absorption and emission taking into account the reabsorption and inhomogeneous distribution of emitting and absorbing atoms. $R = 1$ cm. $\eta(r)$ and $\xi(r)$ are the relative radial distributions of absorbing and emitting atoms. Other symbols are explained in text.

stepwise processes. Chemoionization plays an inessential role, not exceeding 10% of the stepwise ionization rate.

In P striation the stepwise ionization is dominant over the whole striation period. The peak of the direct ionization has a smaller amplitude and larger width than that in S striation. Chemoionization again does not exceed 10% of the total ionization, but reaches about 30% of direct ionization. A significant consequence of the nonlocal electron kinetics is that in S as well as P striation the maximum of the total ionization rate is imposed upon the phase of electron density increase, which is distinctly seen in Figs. 11(b) and 12(b). This circumstance stimulates an ionization wave to propagate from anode to cathode.

V. DENSITY MEASUREMENTS FOR RADIATING AND ABSORBING STATES IN S AND P STRIATIONS

Systematic measurements of the emission and absorption of spectral lines in a neon discharge were performed under the following conditions: the discharge current $i = 5$ mA, the tube radius $R = 1$ cm, and the pressure P was equal to 2 or 3 Torr (Table I). Under these conditions the electron density was considerably smaller than 10^{10} cm^{-3} , and, consequently, the conditions of the experiment were within the theoretical limitations. The peculiarity of excited atom density measurements in striations across the axis of a discharge tube consists in an inhomogeneity of the radiating and absorbing atom distributions in the direction of observation. This circumstance requires a generalization of known methods in order to measure the density of excited atoms [27] taking their inhomogeneous distribution into account.

The scheme of the experimental technique for the measurements of optical characteristics and radiation and absorption of spectral lines in striations is represented in Fig. 13. The image of the discharge tube (1) was projected by the long-focused achromatic objective (3) with iris diaphragm (2) to the entry of a spectrometer (4) with a grating of 2400 grooves/mm. At the monochromator entry there were two crossed slits of 0.1 and 0.5 mm in size. Under the chosen enlargement of the optical system $a:b = 5:1$ the size of the

scanning gap did not make a noticeable contribution to the instrumental profile relative to spatial measurements. The instrumental profile was formed by the finite size of the diaphragm (2) and by aberrations of the objective (3). The resolving ability of the device relative to spatial measurements was about 0.5 mm, which is considerably smaller than the typical spatial scale of striation optical characteristics.

The measurements of the absorption were executed with the help of a radiation source of constant intensity (13), a neon glow discharge without striations at similar pressure and current, powered by a stabilized power source. The radiation from the source was transmitted through the discharge tube with moving striations to the registration circuit. The registration circuit included a photomultiplier in the photon counting mode (5), a pulse generator (6), and a counter (7). Radiation from the same point as that being projected to the spectrometer entry was transmitted to the photomultiplier (9), producing a starting signal, by the radiation conductor (10). The shape and period of striations were controlled by an oscilloscope (11) and frequency the counter (12). The arrangement of the counter (7) allowed us to perform measurements in the following way. The number of impulses was counted during 9 μsec , then the operations of saving the result in a memory cell and choosing the initial value for the next cell were carried out during 1 μsec . Thus, the period of a striation was divided into intervals of 10 μsec and a memory cell was provided for each one. The counting of impulses was carried out during 32 768 striation periods, which was approximately 1 min. for S striation and 2 min for P striation. For these times the parameters of the striations, such as length and frequency, were not changed by more than 0.3%. On completion of counting the results were transmitted to the computer (8) by an RS-232 interface, where the experimental data processing was carried out. The linearity of the registration circuit was controlled in testing experiments. Distortions connected with the nonlinearity of the registration circuit were less than 1%.

The absorption method assumes three signals to be measured: the signal from a discharge tube (1) J_T , the signal from a source (13) J_S , and the signal from a source transmitted through the discharge tube J_{TS} . As an example, in Fig. 14 the results of such measurements are represented for the spectral line 640.2 nm in P striation. Processing of the curves permits one to obtain sufficiently accurate information about the relative densities of radiating and absorbing atoms in different phases of a striation. To obtain the absolute values of the absorbing atom densities, knowledge of reliable values of the transition probabilities or oscillator strengths is required. For radiating atoms, moreover, comparison with a standard source of known spectral intensity is required.

When determining the absorbing atom densities by the technique shown in Fig. 13 it is necessary to consider their inhomogeneous distribution in the direction of observation, which is connected with a radial inhomogeneity of discharge $N_{sk}^{rad}(r) = N_{sk} \eta(r/D)$, where N_{sk} is the absorbing atom density in the state k at the discharge axis, and $\eta(r/D)$ is the relative radial distribution. Later the values $r=0$ and $r=D$ will correspond to the discharge walls.

The output signal of the inhomogeneous discharge under investigation (1) with the effect of the source (13) for the

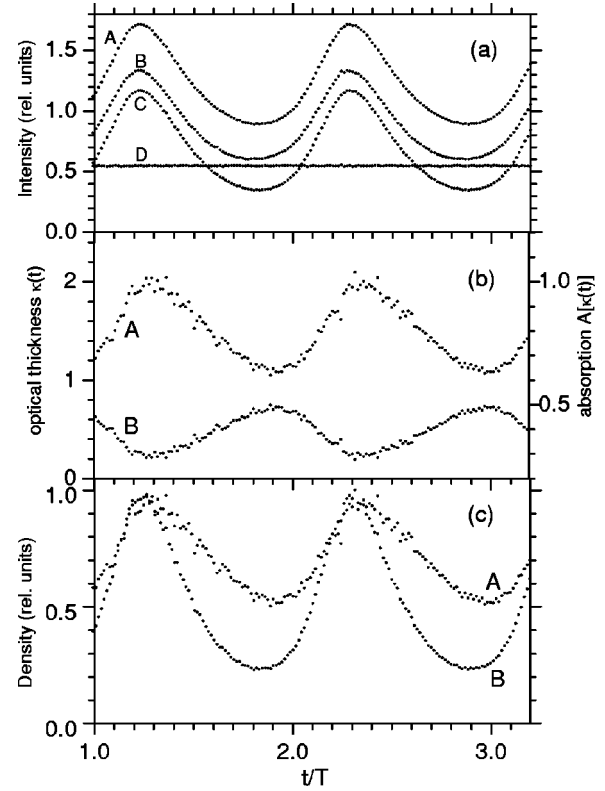


FIG. 14. The measurement result processing to obtain the excited state densities over a striation period. (a) Initial data of the signals from tube $J_T(t)$ (curve C), source $J_S(t)$ (curve D), combined signal from tube and source $J_{TS}(t)$ (curve B), and sum of signals from tube and source $J_T(t) + J_S(t)$ (curve A). The difference between the latter two is connected with absorption. (b) The dependencies of optical density $\kappa(t)$ (curve A) and relative absorption $A[\kappa(t)]$ (curve B) on the normalized time t/T . (c) Distribution of emitting atoms normalized to the maximum value, taking the reabsorption into account, $N_{pj}(t)/N_{pj}^{max}$ (levels $2p^53p$, curve B) and absorbing atoms $N_{sk}(t)/N_{sk}^{max}$ (levels $2p^53s$, curve A).

spectral line ν_{ik} of a transition $pi \rightarrow sk$ can be expressed as

$$J_{TS} = J_T + J_S \int_0^\infty \varepsilon'(\nu) \exp\left(-\int_0^D k(\nu, r) dr\right) d\nu, \quad (11)$$

where J_T is the signal proportional to the radiation flux from the tube (1) integrated over the line contour, J_S is the same from the source (13), and J_{TS} is the total signal obtained by simultaneous observation of radiation from the source (13) and the tube (1), which is generally smaller than the sum of the signals $J_T + J_S$ because of absorption in the tube. $\varepsilon'(\nu)$ is the spectral line profile in the source (13), normalized to unit area, and $k(\nu, r)$ is the absorption coefficient at the frequency ν in the tube (1) at the point r ,

$$k(\nu, r) = \frac{\pi e^2}{mc} f_{ik} N_{sk}^{rad}(r) \varepsilon(\nu), \quad (12)$$

where f_{ik} is the oscillator strength of a corresponding radiative transition, and $\varepsilon(\nu)$ is the spectral line profile in the discharge tube.

The relative absorption value A is defined as

$$A = \frac{J_S + J_T - J_{TS}}{J_S}. \quad (13)$$

To determine the absorbing atom density with the help of a measured value of absorption, it is necessary to consider the relative absorption A as a function of optical density, under assumptions corresponding to the real experiment. The optical density is defined as

$$\kappa = k_0 D \int_0^1 \eta(\rho) d\rho = k_0 D_{eff}, \quad (14)$$

where k_0 is the absorption coefficient in the center of the line at the discharge axis, which is proportional to N_{sk} . The only influence of radial inhomogeneity consists of changing the tube diameter D to the effective tube diameter D_{eff} . For example, when the Bessel distribution of absorbing atoms occurs, $D_{eff} = 0.612D$. The dependence of relative absorption on the optical density can be found by substituting Eq. (11) into Eq. (13), taking Eq. (14) into account:

$$\begin{aligned} A(\kappa) &= 1 - \int_0^\infty \varepsilon'(\nu) \exp\left(-\int_0^D k(\nu, r) dr\right) d\nu \\ &= 1 - \int_0^\infty \varepsilon'(\nu) \exp\left(-\kappa \frac{\varepsilon(\nu)}{\varepsilon(\nu_{ik})}\right) d\nu. \end{aligned} \quad (15)$$

Under the experimental conditions considered the spectral lines from both source and tube are assumed to be identical and to have a Doppler-like profile. Consequently, the value of k_0 is determined by the density of absorbing atoms at the discharge axis N_{sk} according to

$$k_0 = \frac{3\sqrt{\pi \ln 2}}{\Delta \nu_D} \frac{e^2}{mc} N_{sk} f_{ik}. \quad (16)$$

Thus, Eq. (15), taking into account Eqs. (14) and (16), gives the explicit dependence of relative absorption A on the absorbing atom density at the discharge axis N_{sk} . Inverting this function, one can get a value of N_{sk} as a function of the relative absorption directly measured.

To determine the relative densities of radiating atoms it is necessary to introduce a correction for the radiation reabsorption, taking the radial inhomogeneity of the excited atoms into account. The relation between the measured output radiation flux of the discharge tube and the radiation intensity at the tube axis has the form

$$J_T = I_0 dS D \frac{d\Omega}{4\pi} S(\kappa),$$

$$S(\kappa) = \int_0^1 \xi(\rho) d\rho \int_0^\infty \varepsilon(\nu) \exp\left(-D \int_\rho^1 k(\nu, \rho') d\rho'\right) d\nu, \quad (17)$$

where dS is the image of the scanning aperture magnified by $b:a$, $\rho = r/D$, and $\xi(\rho)$ is the relative radial distribution of radiating atoms, $N_{pi}^{rad}(\rho) = N_{pi} \xi(\rho)$. The final result weakly depends on the form of the radial profile. Assuming the profiles of absorption and radiation to be Doppler-like, the function S appears to be

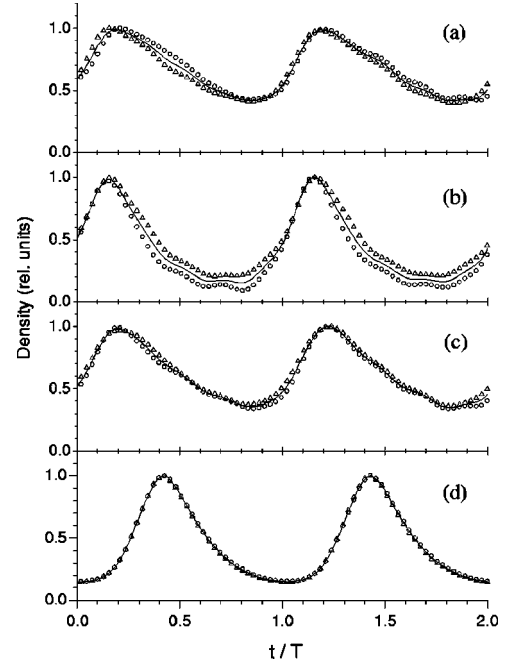


FIG. 15. The density measurements in P striation by different spectral lines. (a)–(c) Densities of absorbing states N_{s2} , N_{s3} , and N_{s4} respectively; triangles, transition $p2 \rightarrow sk$; circles, transition $p4 \rightarrow sk$; solid curve, averaged density. (d) Density of emitting state N_{p2} ; triangles, transition $p2 \rightarrow s5$; circles, transition $p2 \rightarrow s3$; solid curve, averaged density.

$$\begin{aligned} S(\kappa) &= \frac{1}{\sqrt{\pi}} \int_0^1 \xi(\rho) \int_{-\infty}^{\infty} \exp\left(-\omega^2 - k_0 D \exp(-\omega^2)\right) \\ &\quad \times \int_\rho^1 \eta(\rho') d\rho' d\omega d\rho. \end{aligned} \quad (18)$$

The function $S(\kappa)$ in the case of a homogeneous distribution of radiating and absorbing atoms [$\xi(\rho) = 1$, $\eta(\rho) = 1$] is reduced to a Ladenburg-Levy function, introduced for the first time in [28] to consider a correction for the reabsorption in the source.

With such a method one can obtain the excited atom densities over the striation period. An example of experimental data processing is represented in Fig. 14. In Fig. 15(d) the density of the radiating state $p2$ is represented, accounting for the correction for reabsorption. These densities were measured by two spectral lines between the common upper level and different lower levels. The densities of the absorbing atoms, which are also shown in Figs. 15(a)–15(c), were measured by two spectral lines between different upper levels and a common lower level. These results illustrate the accuracy of the relative measurements for the excited atom densities.

Using the above measurement technique the densities of the levels $s3$, $s4$, and $s5$ were obtained in dependence on the phase of the S and P striations. The measurement of the density of the resonance level $s2$ failed because of the small optical length of the plasma for the spectral line of transitions onto this level. The value of the absorption for these transitions did not exceed the noise level.

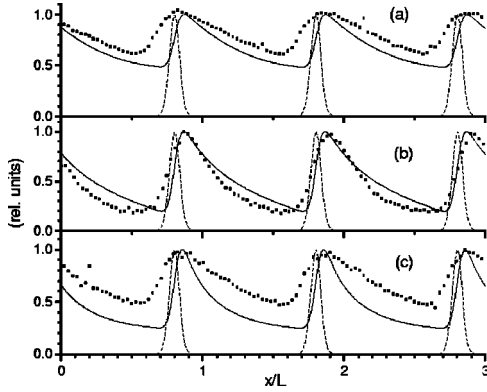


FIG. 16. The comparison of calculated (solid curve) and measured (squares) densities of the levels S_5 (a), S_4 (b), and S_3 (c) of the series $2p^5 3s$, normalized to the maximum value, in dependence on x/L for S striation. Dashed curve is the relative excitation rate of the corresponding level.

VI. COMPARISON OF THEORETICAL AND EXPERIMENTAL RESULTS

The calculated and measured profiles of absorbing atom densities normalized to the maximum are compared in Fig. 16 for S striation and in Fig. 17 for P striation. It is seen from these figures that the calculations of the densities on the basis of nonlocal electron kinetics describe the obtained distributions rather well.

In a P striation (Fig. 17) one can see a good quantitative correspondence between the measured and calculated density profiles for the levels 3P_0 , 3P_1 , and 3P_2 . The resonance level 3P_1 is modulated noticeably more deeply than the metastable levels 3P_0 , 3P_2 , and the level 3P_0 is modulated a little more strongly than the level 3P_2 . This is connected with the differences of the effective lifetimes of different levels, in spite of the intensive intermixing. A similar picture of excited atom distribution over a striation period occurs in S striation (Fig. 16). For the level 3P_1 , the theory describes the experimental data well, and for the levels 3P_0 and 3P_2 the theory gives slightly underestimated results compared to the experimental ones. Apparently, this circumstance is caused by an underestimation of the effective lifetimes used in the theory for these levels. Nevertheless, for S striation qualitative correspondence of the behavior of the densities

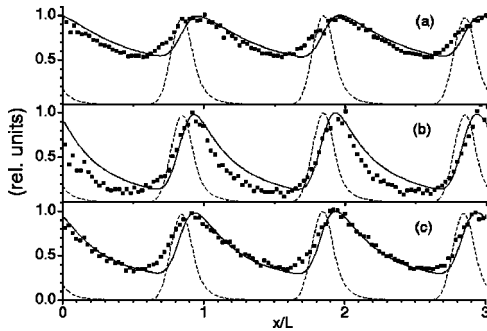


FIG. 17. The comparison of calculated (solid curve) and measured (squares) densities of the levels S_5 (a), S_4 (b), and S_3 (c) of the series $2p^5 3s$, normalized to the maximum value, in dependence on x/L for P striation. Dashed curve is the relative excitation rate of the corresponding level.

TABLE III. The comparison of measured and calculated absolute values of level densities in the system $2p^5 3s$, both the period averaged and maximal (cm^{-3}).

	S striation		P striation	
	Experiment	Theory	Experiment	Theory
$^3P_2(s5)$	max. 2.2×10^{11}	3.3×10^{11}	1.4×10^{11}	2.8×10^{11}
	aver. 1.8×10^{11}	2.2×10^{11}	1.0×10^{11}	2.1×10^{11}
$^3P_1(s4)$	max. 0.54×10^{11}	1.3×10^{11}	4.0×10^{10}	8.6×10^{10}
	aver. 2.5×10^{10}	6.7×10^{10}	1.7×10^{10}	3.9×10^{10}
$^3P_0(s3)$	max. 2.9×10^{10}	4.8×10^{10}	2.2×10^{10}	3.7×10^{10}
	aver. 2.2×10^{10}	2.2×10^{10}	1.4×10^{10}	2.1×10^{10}
$^1P_1(s2)$	max.	1.3×10^{10}		3.7×10^9
	aver.	1.6×10^9		0.84×10^9

over a striation period also occurs.

The difference in the profiles of absorbing atom densities in P and S striations is connected with the appreciable width of the excitation profile in P striation in comparison with that in S striation (dashed curves in Figs. 16 and 17; the full widths at half maximum differ by approximately a factor of 2). The reason for the distinction in the excitation profiles is the distinction of the distribution functions of fast electrons in S - and P -striations.

In Table III the maximal and period averaged absolute values are compared for the measured and calculated densities in the $2p^5 3s$ series of levels. It is seen from Table III that the difference in absolute values given by theory and experiment, as a rule, does not exceed two times, which is evidence of the model's correctness for the distribution function and excited state formation. Such a correspondence should be considered as a satisfactory one, taking into account the experimental errors and uncertainty in elementary process constants.

The experimental data on the level densities in the series $2p^5 3p$ are more accurate than those in the series $2p^5 3s$, as they are based on measurement of the intensity of spectral line radiation but not on absorption. In Fig. 18 the calculated and measured profiles of $p3$ level densities of the series $2p^5 3p$ are compared as an example. A good coincidence of the theoretical and experimental profiles in S and P striations occurs, except in the region near the minimum of lumines-

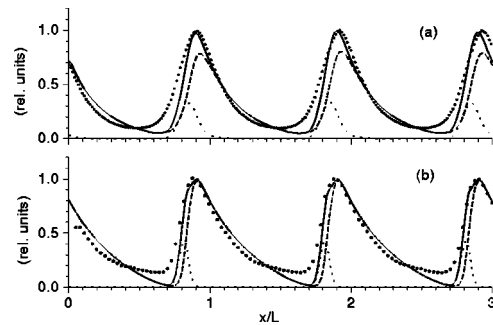


FIG. 18. The comparison of calculated (solid curve) and measured (dots) densities of the level P_3 of the system $2p^5 3s$ of P striation (a) and S striation (b). Dotted curve: relative rate of direct excitation of this level. Dashed curve: relative rate of stepwise excitation of this level.

cence. In this figure the profiles of direct and stepwise excitation of this level are also shown. In both S and P striation the processes of stepwise excitation dominate and determine the spatial profile of the spectral line intensity. The difference between theory and experiment near the minimum of luminescence for the levels $2p^53p$ is connected with the difference in modulation depth for the levels $2p^53s$ involved in stepwise excitation processes.

VII. CONCLUSION

In experimentally measured fields for S and P striations in neon a solution of the Boltzmann kinetic equation is obtained, taking into account elastic and inelastic collisions as well as spatial gradients along the field. The electron distribution functions are calculated in different phases of a striation. Comparison of the calculations and probe measurements of the distribution functions shows that the fundamental peculiarities of electron distribution function formation in a spatially periodic field for electrons of sufficiently small energies are observed in experiment. In accordance with the theory, one maximum in the distribution function for S striation and two maxima for P striation are observed, which move in accordance with the resonance trajectories. On attainment of the excitation potential these maxima abruptly jump to zero kinetic energy, and the movement along the resonance trajectory is repeated. Such a picture of the distribution function formation is a consequence of the electron bunching effect in the resonance fields. The bunching effect under the conditions of the performed experiments is caused by small energy losses in elastic collisions at the striation length.

With the help of the distribution functions obtained, the rates of direct and cascade excitations of the $2p^53s$ series, direct excitations of the $2p^53p$ series, and direct ionization are calculated. The system of balance equations is solved for four metastable and resonance levels $2p^53s$ and ten radiating levels $2p^53p$ taking into account direct, cascade, and step-

wise processes of excitation, processes of direct intermixing by electron collision and collisional-radiational intermixing, stepwise and chemoionization, diffusion of metastable atoms, and resonance radiation loss. The densities of the excited atoms are calculated in different phases of S and P striations. A descriptive model of excitation and ionization processes in striations is constructed. It is shown that the maximum of ionization in striations is imposed upon the phase of the electron density increase, which may cause ionization wave propagation in the anode-to-cathode direction.

Measurements of level densities in the series $2p^53s$ and $2p^53p$ over the striation phases were carried out with high temporal and spatial resolution by methods of emission and absorption. Reabsorption methods were applied to the case of inhomogeneous distribution of radiating and absorbing atoms along the observation direction, which corresponds to the experimental conditions of measurements across the discharge axis.

The comparison performed of the results of calculations and measurements shows good correspondence between the experiment and theory. This circumstance demonstrates the correctness of the formation model of the distribution function in the high-energy part of the spectrum and the densities of excited levels in the framework of nonlocal kinetics. Attempts to describe the experimental results in the framework of local kinetics when the degree of field modulation reaches 94% and the value of the reduced field in striations reaches the magnitude $(E/p)_{max} \sim 4.6$ V/(cm torr) will obviously fail.

Thus it is possible to state that both slow and fast electrons are sufficiently well described in the framework of nonlocal kinetics, which is proved by comparison of the theory and the probe and spectroscopic experiments.

ACKNOWLEDGMENTS

The work was partially supported by Project No. SFB 198/96 and Deutscher Akademischer Austauschdienst.

-
- [1] A. V. Nedospasov, Usp. Fiz. Nauk **94**, 439 (1968) [Sov. Phys. Usp. **11**, 174 (1968)].
 - [2] L. Pekarek, Usp. Fiz. Nauk **94**, 463 (1968) [Sov. Phys. Usp. **11**, 188 (1968)].
 - [3] N. L. Oleson and A. W. Cooper, Adv. Electron. Electron Phys. **24**, 155 (1968).
 - [4] T. Ruzicka and K. Rohlena, Czech. J. Phys., Sect. B **22**, 906 (1972).
 - [5] T. Ruzicka and K. Rohlena, Czech. J. Phys., Sect. B **25**, 660 (1975).
 - [6] T. Ruzicka, K. Rohlena, and L. Pekarek, Phys. Lett. **40A**, 3, 239 (1972).
 - [7] H. Beuder and K. Muller, Z. Phys. **263**, 299 (1973).
 - [8] H. Lergon and K. Muller, Z. Phys. **268**, 157 (1974).
 - [9] L. D. Tsendin, Fiz. Plasmy **8**, 400 (1982) [Sov. J. Plasma Phys. **8**, 228 (1982)].
 - [10] Yu. B. Golubovskii, I. A. Porokhova, J. Behnke, and V. O. Nekutchaev, J. Phys. D **31**, 2447 (1998).
 - [11] Yu. B. Golubovskii, V. O. Nekutchaev, N. S. Ponomarev, and I. A. Porokhova, Zh. Tekh. Fiz. **67**, 17 (1997) [Tech. Phys. **42**, 997 (1997)].
 - [12] F. Sigeneger and R. Winkler, Contrib. Plasma Phys. **36**, 551 (1996).
 - [13] F. Sigeneger and R. Winkler, Plasma Chem. Plasma Process. **17**, 1 (1997).
 - [14] F. Sigeneger, Yu. B. Golubovskii, I. A. Porokhova, and R. Winkler, Plasma Chem. Plasma Process. **18**, 153 (1998).
 - [15] Yu. B. Golubovskii, V. A. Maiorov, I. A. Porokhova, and J. Behnke, J. Phys. D **32**, 1391 (1999).
 - [16] A. B. Stewart, J. Appl. Phys. **27**, 911 (1956).
 - [17] Yu. B. Golubovskii, V. O. Nekutchaev, and I. A. Porokhova, in *Electron Kinetics and Applications of Glow Discharges*, Vol. 367 of *NATO Advanced Study Institute Series B: Physics*, edited by L. D. Tsendin and U. Kortshagen (Plenum, New York, 1999), p. 137.
 - [18] M. Hayashi (private communication).
 - [19] L. A. Vainshtein and L. A. Minaeva, Zh. Prikl. Spektrosk. **9**, 60 (1968).

- [20] L. A. Vainshtein, I. I. Sobelman, and E. A. Yukov, *Cross Sections of Excitation of Atoms and Ions by Electrons* (Nauka, Moscow, 1973).
- [21] T. Holstein, Phys. Rev. **72**, 1212 (1947); **83**, 1159 (1951).
- [22] L. M. Biberman, Zh. Eksp. Teor. Fiz. **17**, 416 (1947).
- [23] A. Phelps, Phys. Rev. **114**, 1011 (1959).
- [24] W. L. Wiese, N. W. Smith, and B. M. Miles, *Atomic Transition Probabilities*, Natl. Bur. Stand. (U.S.) Circ. No. NSRDS-NBS 22 (U.S. GPO, Washington, DC, 1969), Vol. 1.
- [25] V. A. Ivanov, J. Phys. B **31**, 1765 (1998).
- [26] V. M. Alexandrov *et al.*, Plasma Sources Sci. Technol. **5**, 523 (1996).
- [27] S. Frish, *Optical Spectra of Atoms* (State Press of Phys. Mat. Lit., Moscow, 1963).
- [28] L. Ladenburg and S. Levy, Z. Phys. **65**, 189 (1930).